Inference in hydrology from entropy balance considerations

Stefan J. Kollet

IBG-3, Institute for Bio- and Geosciences, Research Centre Jülich, Jülich, Germany
Centre for High-Performance Scientific Computing in Terrestrial Systems, Geoverbund ABC/J, Germany

Correspondence to: S. Kollet (s.kollet@fz-juelich.de)

Abstract

In this study, the method of inference of macroscale potentials, forces and exchange coefficients for variably saturated flow is outlined based on the entropy balance. The theoretical basis of the method of inference is the explicitly calculation of the internal entropy production from microscale flux-force relationships using e.g. hyper-resolution variably saturated groundwater flow models. Emphasis is placed on the two-scale nature of the entropy balance equation that allows incorporating simultaneously movement equations at the micro- and macroscale. The method is demonstrated with simple hydrologic cross-sections at steady state and cyclic sources/sinks at dynamic equilibrium, and provides a thermodynamic point of view of upscaling in variably saturated groundwater flow. The current limitations in the connection with observable variables and predictive capabilities are discussed, and some perspectives for future research are provided.

Introduction

The current earth sciences literature suggests that entropy balance considerations were mainly applied in the context of optimality and self-organization. This is because theories of optimality and self-organization are appealing when dealing with complex non-linear systems, because of their apparent usefulness in interpreting interactions of gradients and fluxes and in quantifying (predicting) systems' states and uncertainties. In this context, the entropy balance received attention, because of its physics-based foundation in non-equilibrium thermodynamics and potential connection with information theory (e.g., Dewar 2003, Koutsoyiannis 2014). The entropy balance appears to be useful in applications to hydrologic (e.g., Zehe et al. 2013, Ehret et al. 2014), ecohydrologic (e.g., Dewar 2010, Miedziejko and Kedziora 2014, del Jesus et al. 2012), and atmospheric sciences (e.g., Paillard and Herbert 2013), and in general to open complex nonlinear thermodynamic systems (Abe and Okuyama 2011).

The entropy balance states that in an open system, the change in entropy equals the internal production of entropy minus the divergence of the entropy current. A dynamic equilibrium or steady state is obtained, when entropy production inside (due to e.g. flow processes of heat and water) equals the divergence of the entropy current i.e. the entropy exchange with the outside. Note also, dynamic equilibrium refers to a state of stationarity in the statistical sense. Optimality of the dynamic equilibrium may be achieved, because the gradient, which drives the flux and, thus the production of entropy, is reciprocally depleted by the same flux (Kleidon et al. 2013).

In hydrology, the entropy balance has been applied to conceptual problems based on the overarching rational that entropy production is maximized (maximum entropy production, MEP) in obtaining a state of dynamic equilibrium by optimizing the fluxes and gradients in competition via an adjustment of some (non-)linear exchange coefficient. There have been some studies demonstrating, how entropy production can be optimized as a function of an exchange coefficient to obtain a system's state at which entropy production is indeed at its maximum. In hydrology, there are quite a few examples of the

application and discussion of the MEP principle (e.g., Ehret et al. 2014, Westhoff et al. 2014, Kleidon and Schymanski 2008) also in connection with data (e.g., Zehe et al. 2013). However, its validity and applicability to hydrologic systems is still in question (Westhoff and Zehe 2013).

Often the entropy balance has been applied at steady state with simple bucket models, which are well-mixed (i.e. without internal gradients). For example, Porada et al. (2011) performed a detailed entropy production analysis of the land surface hydrologic cycle including the shallow vadose zone assuming vertical equilibrium of the soil bucket model. Applying linear bucket models without considering internal gradients, Kleidon and Schymanski (2008) showed that if the natural system possesses enough degrees of freedom, in case of steady state, the system will tend towards a certain exchange coefficient, when entropy production is maximized. For similar bucket models, Westhoff et al. (2014) demonstrated the impact of periodic boundary forcing on entropy production, which may result in more than one maximum for unique values of the exchange coefficient at dynamic equilibrium. Interestingly, these studies did not calculate the internal entropy production explicitly; entropy production was estimated indirectly from the exchange with the outside (i.e. the divergence of the entropy current).

Schymanski et al. (2010) recognized the potential in explicitly estimating the internal entropy production using a simple microscale Klausmeier model (Klausmeier 1999), which is based on coupled equations of moisture and biomass and is able to produce vegetation patterns, in order to optimize effective values of a simple two-box model. This study highlights an interesting aspect of entropy balance considerations related to the inference of upscaled effective parameters and state variables to represent subgrid scale variability in coarse scale (macroscale) models. Thus, ultimately, the appeal of the entropy balance maybe the inference of upscaled or effective exchange coefficients and forces/gradients, which may be used to quantitatively describe the complex system without the explicit knowledge about microscopic details (Dewar 2009). In this context, a popular example is gas diffusion, which can be captured by an

inferred, macroscopic diffusion coefficient and gradient instead of honoring the motion and interactions of individual molecules.

In this study, the method of inference of effective hydrologic exchange coefficients, potentials and forces is outlined using the entropy balance equation in applications to simple hydrologic cross-sections. The following sections provide the basic theory with an emphasis on the two-scale nature of the entropy balance, and the application to the hydrologic cross-sections with ensuing discussion and conclusions.

Basic theory and the two-scale nature of the entropy balance

The theory outlined in Kondepudi and Prigogine (2015) is applied to the problem of variably saturated groundwater flow at constant temperature. Based on conservation of energy (and the balance equation for concentrations, which is not required in this analysis) Kondepudi and Prigogine (2015) write the entropy balance as follows

$$s' + \nabla \cdot J_s = \sigma \qquad (1),$$

where s' ($ML^{-1}T^{-3}K^{-1}$) is the change in the entropy density with time; J_s ($MT^{-3}K^{-1}$) is the entropy current per unit volume; and σ ($ML^{-1}T^{-3}K^{-1}$) is the internal entropy production per unit volume, which is always positive by definition. Thus, the change of entropy density with time of a macroscopic volume depends on the divergence of the entropy current and the internal entropy production.

In the considered case of variably saturated groundwater flow, $J_s = JM/T$, where J($ML^{-2}T^{-1}$) is the mass flow per unit area, M(L^2T^{-2}) is the chemical potential at the macroscale and T (K) is the temperature. Defining q($ML^{-3}T^{-1}$) and f(L^2T^{-2}) as the fluxes and forces at the microscale per unit volume, the divergence of the entropy current and the internal entropy production can be expanded as follows

$$s' + (M/T)(\nabla \cdot J) + J \cdot \left(\nabla (M/T)\right) = \sum qf/T \qquad (2).$$

Equation (2) exhibits the unique characteristics of incorporating two scales: the entropy density change with time and divergence of the entropy current at the macroscale (all terms on the left hand side), and the entropy production at the microscale i.e. the sum of all products of the internal microscopic fluxes and forces (term on the right hand side). Note, in the following, T(K) is omitted in the equations and units, because T= constant in the following derivations.

Performing an entropy balance at true steady state leads to

$$M(\nabla \cdot J) + J \cdot (\nabla M) = \sigma \quad (3)$$

because $s' = 0$. In contrast, performing an entropy balance under the influence of periodic external forcing requires integration over one full forcing cycle at dynamic equilibrium of equation 2 indicated by overbars

$$\overline{M(\nabla \cdot J)} + \overline{J \cdot (\nabla M)} = \bar{\sigma} \quad (4).$$

with $\overline{s'} = 0$ over one full cycle. Both approaches will be applied in the following section, in order to arrive at effective variables at the macroscale.

In order to further emphasize the two-scale nature of equations 1 and 2, movement equations are introduced at the macro- and microscale. At the macroscale, M(L^2T^{-2}) is defined as the sum of the macroscopic pressure potential Ψ (L^2T^{-2}), and gravitational potential gz (L^2T^{-2}), leading to

$$M = \Psi + gz \quad (5);$$

and is, thus, equivalent to the hydraulic head; (∇M) symbolizes a macroscopic force F(L^2T^{-2}) being the difference in the macroscopic chemical potentials

$$(\nabla M) = F = M_{high} - M_{low} \quad (6);$$

and, at the moment, J is defined as a conductance concept

$$J = \lambda F \quad (7),$$

where λ ($ML^{-4}T$) is a conductance coefficient ($\lambda = \rho r_s$, with water density ρ (ML^{-3}) and resistance r_s (TL^{-1})) relating the flux with the force at the macroscale.

At the microscale, the chemical potential μ, (L^2T^{-2}), the mass flux q ($ML^{-3}T^{-1}$) per unit volume and the force f(L^2T^{-2}) are

$$\mu = \psi + gz \quad (8),$$

where ψ (L^2T^{-2}) is the microscale pressure potential;

$$q = \frac{1}{\alpha}\,\rho\,\frac{K}{v}k_r(\psi)\left(\mu_{high} - \mu_{low}\right) \quad (9),$$

where ρ (ML^{-3}) is the density; υ (L^2T^{-1}) is the kinematic viscosity; K is the permeability (L^2), $k_r(\psi)$ (-) is the relative permeability, and α (L^{-2}) is the unit microscopic flow through area; and the microscale force

$$f = \left(\mu_{high} - \mu_{low}\right) \quad (10).$$

Technically, $\sum qf$ is the sum of all fluxes and forces (both always positive, because any flux produces entropy) between all neighboring cells or elements in a microscale, numerical, variably saturated groundwater flow model including any Dirichlet and Neumann boundary conditions.

Thus, the two-scale nature of equation 2 allows to apply different flux-force relationships at the different scales that are the conductance concept at the macroscale (equation 7) and essentially Darcy's law or Richards equation (equation 7) at the microscale. In equation 2, the entropy production serves as an "automatic" spatial and also temporal integrator of the microscale fluctuations. These two characteristics are remarkable. Note, the calculation (integration) of the entropy balance may be performed over the global domain of volume V (L^3) or any subdomain V_i (L^3) thereof.

Method of Inference

The basis of the method of inference is that the internal, microscopic entropy production σ and also the complete entropy balance can be calculated from support scale simulations by implementing the microscale equations 9 and 10 in combination with a continuity equation over the macroscopic domain. In obtaining σ explicitly, one is able to estimate effective potentials, forces and conductance coefficients, at the macroscale (equation 7) from the explicitly resolved fluctuations at the microscale, which are thermodynamically consistent. In order to illustrate the method of inference of macroscale potentials, conductances and forces, a number of illustrative examples based on simple hydrologic profiles are presented applying different boundary conditions and source terms.

Example 1:

Directed at a heat flow example in Kondepudi and Prigogine (2015), a simple cross-section is considered (figure 1) with steady-state, variably saturated groundwater flow, J, from left to right due to Dirichlet boundary conditions on the left M_l, and right M_r, with $M_l > M_r$. Because $\nabla \cdot J = 0$, and $s' = 0$ at steady state, integration of the entropy balance over the cross-section leads to

$$S_i' = \int_0^{L_z} \int_0^{L_x} \sigma(x,z) dx\, dz = L_z \int_0^{L_x} J_x (\nabla_x M) dx \qquad (11a)$$

$$S_i' = L_z J_x (M_l - M_r) = L_z J_x F \qquad (11b),$$

where L_z and L_x (L) are the constant vertical and horizontal extents of the cross-section, respectively; S_i' is the total internal entropy production; and $F = (M_l - M_r)$ is the macroscopic force. Note, in the following, the entropy production integral is simply written as $S_i' = \int \sigma$, and L_z is lumped into the flux $L_z J_x = J$ for convenience.

In case of this simple example, applying $J = \lambda(M_l - M_r)$ from equation 5, one obtains the expression for the effective conductance

$$\lambda = S_i'(M_l - M_r)^{-2} = S_i' F^{-2} \quad (12)$$

and the effective force

$$F = S_i' J^{-1} \quad (13).$$

Thus, one may obtain the true, effective conductance for any kind of heterogeneity (i.e. microscale fluctuations) by explicitly calculating σ and S_i' based on equations 6 and 7 and the macroscopic boundary conditions M_l and M_r. Note, entropy production is simply the sum of the product of the steady state fluxes and incremental forces over the cross-section $S_i' = \int \sigma = \int (\sum qf) = \int \left(\sum \frac{1}{\alpha} \rho \frac{K}{v} k_r(\psi) \left(\mu_{high} - \mu_{low} \right)^2 \right)$, where individual values of qf are calculated with equations 9 and 10 between two adjacent microscale elements in support scale numerical simulations.

Example 2:

This example expands example 1 to steady state groundwater flow including recharge represented by the mass rate Q_s

$$Q_s = \int_0^L (\nabla \cdot J) dx \quad (14),$$

and integration leading to

$$MQ_s + J_l M_l - J_r M_r = S_i' \quad (15).$$

where M is the macroscopic potential of the cross-section.

176 The general expression for the macroscopic potential of the cross-section is

177 $$M = {Q_s}^{-1}(S_i' - (J_l M_l - J_r M_r)) \quad (16).$$

178 In this example, three special cases are considered, namely $J_l = 0$, $J_l < 0$, and $J_l > 0$. In case of $J_l = 0$

179 (figure 2), there is a no-flow boundary condition on the left side resulting in $J_r = Q_s$ and, thus

180 $$M = S'_{i,J_l=0}{Q_s}^{-1} + M_r \quad (17)$$

181 $$F = (M - M_r) = S'_{i,J_l=0}{Q_s}^{-1} \quad (18)$$

182 where the subscript indicates the respective case for the left boundary flux.

183 With equation 7 and $J_r = Q_s = J$ follows for the conductance coefficient

184 $$\lambda = S'_{i,J_l=0}F^{-2} \quad (19).$$

185 For $J_l < 0$ (figure 3), the symmetric case is considered, where the potentials at the boundaries are equal

186 $(M_l = M_r = M_b)$ and Q_s is uniform over the profile $(-J_l = J_r = Q_s/2)$ leading to

187 $$MQ_s - 1/2Q_s M_l - 1/2Q_s M_r = S'_{i,J_l<0} \quad (20a).$$

188 $$Q_s(M - (M_l + M_r)/2) = S'_{i,J_l<0} \quad (20b).$$

189 $$Q_s(M - M_b) = S'_{i,J_l<0} \quad (20c)$$

190 and ultimately for the macroscopic potential

191 $$M = S'_{i,J_l<0}{Q_s}^{-1} + M_b \quad (21).$$

192 $$F = (M - M_b) = S'_{i,J_l<0}{Q_s}^{-1} \quad (22)$$

193 and

$$\lambda = S'_{i,J_l<0} F^{-2} \quad (23)$$

Note, M and F reflect values for each of the two half-spaces separated by a no-flow boundary condition e.g. $F = \left(S'_{i,J_l<0}/2\right)(Q_s/2)^{-1}$, which is true for a homogeneous profile only and is equivalent to the case $J_l < 0$ above. The entropy production is calculated also with

$$S'_{i,J_l<0} = \int \sigma = \int (\sum qf) = \int \left(\sum \frac{1}{\alpha}\, \rho \frac{K}{v} k_r(\psi)\left(\mu_{high} - \mu_{low}\right)^2\right).$$

For a heterogeneous profile and/or $M_l > M_r$ (figure 4) i.e. when there is no symmetry

$$MQ_s - J_l M_l - J_r M_r = S'_{i,J_l<0} \quad (24).$$

Thus, the effective potential of the cross section may be obtained from

$$M = {Q_s}^{-1}\left(S'_{i,J_l<0} + J_l M_l + J_r M_r\right) \quad (25)$$

Additionally, expressions can be obtain for the conductance coefficients in the exchange with the left and right boundary conditions that are

$$\lambda_l = \left(MQ_s - S'_{i,J_l<0} - J_r M_r\right)(F_l M_l)^{-1} \quad (26a)$$

$$\lambda_r = \left(MQ_s - S'_{i,J_l<0} - J_l M_l\right)(F_r M_r)^{-1} \quad (26b).$$

where the macroscale forces $F_r = M - M_r$ and $F_l = M - M_l$ result from the differences between M and M_l, M_r with M following from equation 25. Again, entropy production is calculated with

$$S'_{i,J_l<0} = \int \sigma = \int (\sum qf) = \int \left(\sum \frac{1}{\alpha}\, \rho \frac{K}{v} k_r(\psi)\left(\mu_{high} - \mu_{low}\right)^2\right).$$

For $J_l > 0$ (figure 5), the entropy balance is

$$MQ_s + J_l M_l - J_r M_r = S'_{i,J_l>0} \quad (27)$$

and the macroscopic potential is

$$M = {Q_s}^{-1}\left(S'_{i,J_l>0} - J_l M_l + J_r M_r\right) \quad (28)$$

With $Q_s = J_r - J_l$ follows

$$J_l(M_l - M) + J_r(M - M_r) = S'_{i,J_l>0} \quad (29)$$

Thus, two conductances can be obtained, which are

$$\lambda_l = \left(S'_{i,J_l>0} - J_r(M - M_r)\right) {F_l}^{-2} \quad (30)$$

$$\lambda_r = \left(S'_{i,J_l>0} - J_l(M_l - M)\right) {F_r}^{-2} \quad (31)$$

with the macroscopic forces $F_l = (M_l - M)$ and $F_r = (M - M_r)$. In this example, two additional conductances can be obtained for the subdomains separated by the dividing streamline due to recharge shown in figure 5 that are

$$\lambda_{Q_s} = \left(S'_{i,J_l>0} - J_l(M_l - M_r)\right) {F_{Q_s}}^{-2} \quad (32)$$

$$\lambda_{l,r} = \left(S'_{i,J_l>0} - Q_s(M - M_r)\right) {F_{l,r}}^{-2} \quad (33)$$

with $J_r = J_l + Q_s$, and the macroscale forces $F_{Q_s} = (M - M_r)$ and $F_{l.r} = (M_l - M_r)$. In the domain, the entropy production is calculated also with

$$S'_{i,J_l>0} = \int \sigma = \int (\sum qf) = \int \left(\sum \frac{1}{\alpha}\, \rho \frac{K}{v} k_r(\psi)\left(\mu_{high} - \mu_{low}\right)^2\right).$$

Example 3:

In this example, a no-flow boundary condition on the left is considered resembling a hillslope with a no-flow boundary along a hypothetical ridge on the left side, and a Dirichlet boundary condition along a hypothetical stream on the right side. Now, a source/sink $Q_s(x,t)$ varies periodically in space and time

(periodically varying recharge/discharge). In this case, equation 2 needs to be solved for the different variables and integrated over one complete cycle at dynamic equilibrium.

Note, again $\int_0^L \nabla \cdot J dx = Q_s$, because there is a macroscopic, transient source/sink in the domain, therefore, after integration along the cross-section, the entropy balance reads

$$S' + MQ_s - J_r M_r = S_i' \tag{34}$$

where S' is the entropy change rate. After time integration over one full cycle at dynamic equilibrium, $\overline{Q_s} = 0$ and $\overline{S'} = 0$, the effective macroscopic potential of the cross-section due to the periodic varying source/sink is

$$\bar{M} = \overline{(S_i' + J_r M_r - S')Q_s^{-1}} \tag{35a}$$

or

$$\bar{M} = \mathrm{cov}(S_i', Q_s^{-1}) + \overline{S_i'}\,\overline{Q_s^{-1}} + M_r\left(\mathrm{cov}(J_r, Q_s^{-1}) + \overline{J_r}\,\overline{Q_s^{-1}}\right) + \mathrm{cov}(S', Q_s^{-1}) \tag{35b}$$

Recognizing that $J_r = \int_0^L (Q_s - \Theta')dx$, where Θ' is the macroscopic mass change rate of the cross-section, one obtains for the effective force

$$\bar{F} = \overline{(S_i' - \Theta M_r - S')Q_s^{-1}} \tag{36a}$$

or

$$\bar{F} = \mathrm{cov}(\sigma, Q_s^{-1}) + \bar{\sigma}\,\overline{Q_s^{-1}} - M_r \mathrm{cov}(\Theta', Q_s^{-1}) + \mathrm{cov}(s', Q_s^{-1}) \tag{36b}$$

with $\overline{\Theta} = 0$; and for the effective conductance

$$\bar{\lambda} = \overline{(S_i' - \Theta' \mathrm{M} - S')F^2} \tag{37a}$$

or

$$\bar{\lambda} = \mathrm{cov}(S_i', F^2) + \overline{S_i'}\,\overline{F^2} - \mathrm{cov}(\Theta' \mathrm{M}, F^2) + \overline{\Theta' M}\,\overline{F^2} + \mathrm{cov}(S', F^2) \quad (37b)$$

with $J_r = \lambda F = \lambda(M - M_r)$.

Apparently, on the right hand side of equations 35, 36, and 37 all terms may be calculated from the numerical simulations except $S' = \int s'$ and therefore also $\mathrm{cov}(S', Q_s^{-1})$, because $S'$and M is not known in equation 34 (note, S_i' is calculated explicitly). However, S' may actually be calculated from the microscale variables, which is demonstrated with a discrete example depicted in the schematic in figure 6.

In this schematic, there are three microscale elements with sources/sinks in each individual element (q_l, q_c, q_r) and a constant potential boundary condition on the right (μ_b). For each individual element the entropy balance is

$$s_l' + q_l\mu_l - q_{l,c}\mu_{l,c} = \sum q_l f_l = q_{l,c}\left(\mu_l - \mu_{l,c}\right) \quad (38a)$$

$$s_c' + q_c\mu_c + q_{l,c}\mu_{l,c} - q_{c,r}\mu_{c,r} = \sum q_c f_f = q_{l,c}\left(\mu_{l,c} - \mu_c\right) + q_{c,r}\left(\mu_c - \mu_{c,r}\right) \quad (38b)$$

$$s_r' + q_r\mu_r + q_{c,r}\mu_{c,r} - q_b\mu_b = \sum q_r f_r = q_{c,r}\left(\mu_{c,r} - \mu_r\right) + q_b(\mu_r - \mu_b) \quad (38c)$$

where the fluxes and potentials with the subscript l,c and c,r are valid at the element interfaces. The terms on the right hand side i.e. the entropy production for each element encompass the fluctuations in the flux-force relationships between the element's interior and the element boundaries. Summation of the individual balance equations leads to the total balance

$$s' + q_l\mu_l + q_c\mu_c + q_r\mu_r - q_b\mu_b = \sigma = q_{l,c}(\mu_l - \mu_c) + q_{c,r}(\mu_c - \mu_r) + q_b(\mu_r - \mu_b) \quad (39).$$

Note, on the left hand side, all the interface terms disappear and only the source and boundary terms remain, equivalent to the macroscale balance in equation 34. Equation 38 is the entropy balance equation for the system depicted in figure 6.

Any changes in the entropy of the system with time are due to transient effects that cancel out at dynamic equilibrium $\overline{s'} = 0$. In order to demonstrate this, substitution of $q_{l,c} = (q_l - \theta'_l)$, $q_{c,r} = (q_l - \theta'_l) + (q_c - \theta'_c)$, and $q_b = (q_l - \theta'_l) + (q_c - \theta'_c) + (q_r - \theta'_r)$ for the interface fluxes on the right hand side in equation 38 leads to

$$s' + q_l\mu_l + q_c\mu_c + q_r\mu_r - q_b\mu_b =$$

$$(q_l - \theta'_l)\mu_l + (q_c - \theta'_c)\mu_c + (q_r - \theta'_r)\mu_r - q_b\mu_b \quad (40)$$

which demonstrates continuity in case of true steady state $\theta'_l = \theta'_c = \theta'_r = 0$, and shows that any e.g. positive mass storage change θ' over the microscopic volume leads to negative change in entropy and vice versa. Note, the entropy production is still always positive. Thus, S' and can be evaluated by applying equation 39 to microscale simulations.

A special case may be considered, in which the system depicted in figure 6 is also closed on the right side resulting in a sole exchange with the surroundings via the periodic source/sink $Q_s(t)$. This would be equivalent to a profile with a discharge area in the center and the assumption of symmetry shown in the schematic in figure 7. The requirement again is that $\overline{Q_s} = 0$ over one full cycle at dynamic equilibrium. Then e.g. equation 35 simplifies to

$$\bar{M} = \overline{(S'_i - S')Q_s^{-1}} \quad (41a)$$

or

$$\bar{M} = \mathrm{cov}(\Delta S', Q_s^{-1}) + \bar{S}'_i\overline{Q_s^{-1}} \quad (41a)$$

with $\Delta S' = S'_i - S'$.

Discussion

The major advantage of the proposed inference theory is the estimation of macroscopic variables that are thermodynamically consistent with the microscale fluctuations. This is discussed in the context of the simple example 1 interpreting the entropy current $J_s = JM$ as an advective potential flux. Because J is constant and $M_l > M_r$, the entropy current leaving the domain on the right side is smaller than the entropy current entering the domain on the left side. This is due to dissipation in the interior of the domain resulting into the production of entropy S_i'. In hydrology, the dissipation is simulated using Darcy's law and Richards equation at the support (here microscopic) scale, where all dissipative processes are lumped in the hydraulic conductivity representing the flow resistance. Thus, at the macroscale the derived conductance λ is thermodynamically consistent if one accepts e.g., Darcy's law as a valid parameterization of the internal dissipative processes.

Equations 12 and 13 have not been applied before in the context of hydrology. While the equations illustrate the basic idea for the simplest case of a Darcy experiment, one may argue that the insight gained from this example is rather limited, because λ could have been obtained from the known flux-force relationship and the conductance equation (one unknown λ with one equation 7). Examples 2 and 3, on the other hand, clearly illustrate the advantage, because the macroscale potential M (and therefore F),which are needed to obtain λ are not known in these examples. Thus, one is left with two unknowns λ and F, and only one equation (the conductance equation 7). In the proposed theory, the entropy balance provides the second equation to solve for the two unknowns at the cost of explicitly calculating the internal entropy production $S_i' = \int \sigma = \int (\sum qf) = \int \left(\sum \frac{1}{\alpha} \rho \frac{K}{v} k_r(\psi) \left(\mu_{high} - \mu_{low} \right)^2 \right)$, and at the benefit of thermodynamic consistency. This is the central message of the proposed method of inference, which utilizes S_i' as a spatial and also temporal integrator.

It is important to emphasize that one can also obtain, in an ad hoc fashion, the forces and conductance coefficients for any sub-domain V_i of the global domain with volume V. For example, in order to obtain the macroscale potential in the center of the profile of example 1, one arrives at

$$M_c = M_l - J^{-1} \int_{V_i} \sigma dV_i \qquad (42).$$

Thus, from $\int_{V_i} \sigma dV_i$ estimates, one is able to obtain macroscale variables over a hierarchy of scales for different hydrologic configurations similar to the simple examples provided above.

Under purely saturated groundwater flow conditions, the estimates of macroscale variables can be used directly for predictions, because λ is constant for the same flow geometries, which is trivial, but important to realize. In case of variably saturated flow and transient conditions (when the flow geometry changes), λ is of course not constant and S_i' will depend in an unknown, non-linearly fashion on the flux J and its variability (example 3), which apparently limits the usefulness of the proposed approach. However, universal relationships of $S_i'(J)$ and $\mathrm{cov}(S_i', J^{-1})$ can perhaps be obtained from a series of numerical experiments under characteristic hydrologic configurations.

This also brings up the question, whether one is able to establish a connection of the proposed theory with observations of real-world systems. Obviously, S_i' and S' can not be measured directly in the field utilizing independent experiments, which could, in turn, be used to derive macroscopic forces from flux observations that are more readily available. Thus, utilizing the entropy balance for estimating macroscopic field variables and ensuing predictions appears limited at this point. Yet, this study suggests to explore relationships of measurable field variables and S_i' utilizing numerical experiments, in future. In turn, under certain conditions, estimates of S_i' from measurable quantities may be possible. With the help of the extended example 1, this is discussed below.

Assuming a time varying force i.e. Dirichlet boundary conditions, temporal integration of equation 11 over one full cycle at dynamic equilibrium yields

$$\overline{S_i'} = \overline{JF} \quad (43)$$

Inserting the conductance equation into equation 43 under saturated, linear groundwater flow conditions with the assumption of only small changes in the flow geometry (λ is constant) leads to

$$\overline{S_i'} = \lambda^{-1}\overline{J^2} = \lambda^{-1}[\mathrm{var}(J) + \bar{J}^2] \quad (44).$$

Thus, entropy production is related inversely to λ, linearly with J, and power two with $\bar{J}$. If an estimate of λ is available, $\overline{S_i'}$ can be calculated from observations of J. In the more realistic case of variably saturated groundwater flow and/or varying flow geometry, equation 44 changes to

$$\overline{S_i'} = \overline{\lambda^{-1}J^2} = \mathrm{cov}(\lambda^{-1}, J^2) + \overline{\lambda^{-1}}\bar{J}^2 \quad (45).$$

illustrating the same dependence of $\overline{S_i'}$ on $\bar{\lambda}$ and $\bar{J}$ as before. The unknown covariance $\mathrm{cov}(\lambda^{-1}, J^2)$ may potentially be estimated from numerical experiments.

Summary and conclusions

In this study, the method of inference based on the entropy balance equation was introduced. The theoretical basis is the explicit calculation of the internal microscale entropy production, which is used in the balance equation to solve for macroscale potentials, forces and fluxes. The proposed method was illustrated with simple hydrologic cross-sections of stead-state, variably saturated groundwater flow and a periodic source/sink at dynamic equilibrium.

The entropy balance equation is remarkable, because the equation unifies the macro- and microscale in one equation allowing the simultaneous application of two different movement equations that are the

conductance equation at the macroscale and Darcy's law/Richards equation at the microscale, in this study. The derivations lead to expressions for macroscale variables that are a function of the entropy production (i.e. the internal fluctuations of the microscale flux-force relationships) and are, thus, thermodynamically consistent. Therefore, the derivation provides a different theoretical point of view of variably saturated groundwater flow and new approaches for obtaining effective macroscale variables. The discussion suggests that these may be derived consistently for a hierarchy of scales. With the advent of high-performance computing in hydrology, there is strong potential for additional insight from hyper-resolution numerical experiments to explicitly calculate the internal entropy production. For example, existing and new averaging and uspcaling laws may be tested and derived using series of numerical experiments with e.g. varying subsurface heterogeneity configurations, and boundary conditions. These experiments may also be useful in deriving new movement equations at the macroscale replacing empirical, calibrated parameterizations and regionalization approaches.

Thus, the appeal of the proposed method is mainly theoretical at this point, providing a thermodynamics perspective of inference in hydrology. The connection to real-world observations needs to be established in future, also with the help of numerical simulations. In the provided theoretical setting, the usefulness of the method for predictions is evident from the simple examples provide here, however, for real-world predictions this remains to be demonstrated.

References

Dewar, R. (2003) Information theory explanation of the fluctuation theorem, maximum entropy production and self-organized criticality in non-equilibrium stationary states. Journal of Physics a-Mathematical and General 36(3), 631-641.

Koutsoyiannis, D. (2014) Entropy: From Thermodynamics to Hydrology. Entropy 16(3), 1287-1314.

379 Zehe, E., Ehret, U., Blume, T., Kleidon, A., Scherer, U. and Westhoff, M. (2013) A thermodynamic
380 approach to link self-organization, preferential flow and rainfall-runoff behaviour. Hydrology and Earth
381 System Sciences 17(11), 4297-4322.

382 Ehret, U., Gupta, H.V., Sivapalan, M., Weijs, S.V., Schymanski, S.J., Bloschl, G., Gelfan, A.N., Harman, C.,
383 Kleidon, A., Bogaard, T.A., Wang, D., Wagener, T., Scherer, U., Zehe, E., Bierkens, M.F.P., Di Baldassarre,
384 G., Parajka, J., van Beek, L.P.H., van Griensven, A., Westhoff, M.C. and Winsemius, H.C. (2014) Advancing
385 catchment hydrology to deal with predictions under change. Hydrology and Earth System Sciences 18(2),
386 649-671.

387 Dewar, R.C. (2010) Maximum entropy production and plant optimization theories. Philosophical
388 Transactions of the Royal Society B-Biological Sciences 365(1545), 1429-1435.

389 Miedziejko, E.M. and Kedziora, A. (2014) Impact of plant canopy structure on the transport of ecosystem
390 entropy. Ecological Modelling 289, 15-25.

391 del Jesus, M., Foti, R., Rinaldo, A. and Rodriguez-Iturbe, I. (2012) Maximum entropy production, carbon
392 assimilation, and the spatial organization of vegetation in river basins. Proceedings of the National
393 Academy of Sciences of the United States of America 109(51), 20837-20841.

394 Paillard, D. and Herbert, C. (2013) Maximum Entropy Production and Time Varying Problems: The
395 Seasonal Cycle in a Conceptual Climate Model. Entropy 15(7), 2846-2860.

396 Abe, S. and Okuyama, S. (2011) Similarity between quantum mechanics and thermodynamics: Entropy,
397 temperature, and Carnot cycle. Physical Review E 83(2).

398 Kleidon, A., Zehe, E., Ehret, U. and Scherer, U. (2013) Thermodynamics, maximum power, and the
399 dynamics of preferential river flow structures at the continental scale. Hydrology and Earth System
400 Sciences 17(1), 225-251.

401 Westhoff, M.C., Zehe, E. and Schymanski, S.J. (2014) Importance of temporal variability for hydrological
402 predictions based on themaximum entropy production principle. Geophysical Research Letters 41(1), 67-
403 73.

404 Kleidon, A. and Schymanski, S. (2008) Thermodynamics and optimality of the water budget on land: A
405 review. Geophysical Research Letters 35(20).

406 Westhoff, M.C. and Zehe, E. (2013) Maximum entropy production: can it be used to constrain conceptual
407 hydrological models? Hydrology and Earth System Sciences 17(8), 3141-3157.

408 Porada, P., Kleidon, A. and Schymanski, S.J. (2011) Entropy production of soil hydrological processes and
409 its maximisation. Earth System Dynamics 2(2), 179-190.

410 Schymanski, S.J., Kleidon, A., Stieglitz, M. and Narula, J. (2010) Maximum entropy production allows a
411 simple representation of heterogeneity in semiarid ecosystems. Philosophical Transactions of the Royal
412 Society B-Biological Sciences 365(1545), 1449-1455.

413 Klausmeier, C.A. (1999) Regular and irregular patterns in semiarid vegetation. Science 284(5421), 1826-
414 1828.

415 Dewar, R.C. (2009) Maximum Entropy Production as an Inference Algorithm that Translates Physical
416 Assumptions into Macroscopic Predictions: Don't Shoot the Messenger. Entropy 11(4), 931-944.

417 Kondepudi, D. and Prigogine, I. (2015) Modern Thermodynamics: From Heat Engines to Dissipative
418 Structures, 2nd Edition. Modern Thermodynamics: From Heat Engines to Dissipative Structures, 2nd
419 Edition, 1-523.

420

421

Figures

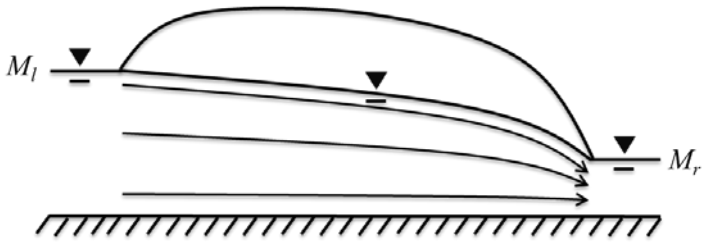

Figure 1. Schematic of a simple profile with Dirichlet boundary conditions on the right and left (M_r, M_r) and steady state variably saturated flow. In the theory, the vertical and horizontal extents of the cross-section are assumed to be constant.

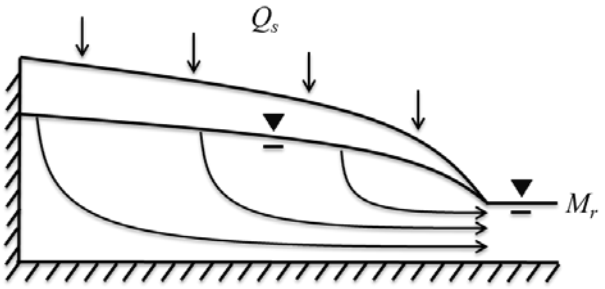

Figure 2. Schematic of a simple profile with a Dirichlet boundary condition on the right (M_r), a no-flow boundary condition on the left, a constant source (Q_s), and steady state variably saturated groundwater flow. In the theory, the vertical and horizontal extents of the cross-section are assumed to be constant.

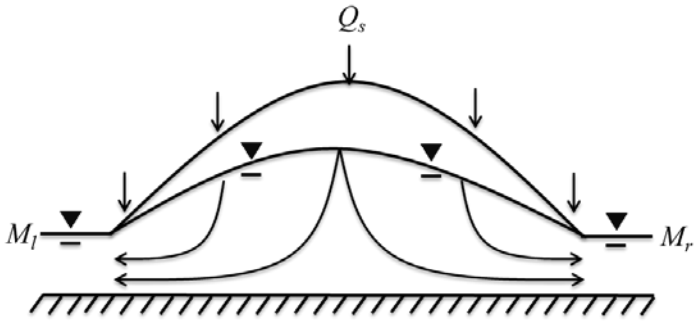

Figure 3. Schematic of a simple profile with Dirichlet boundary conditions on the right and left(M_r, M_r) a constant source (Q_s), and steady state variably saturated groundwater flow. In this symmetric case, there exist a water divide in the center of the domain. In the theory, the vertical and horizontal extents of the cross-section are assumed to be constant.

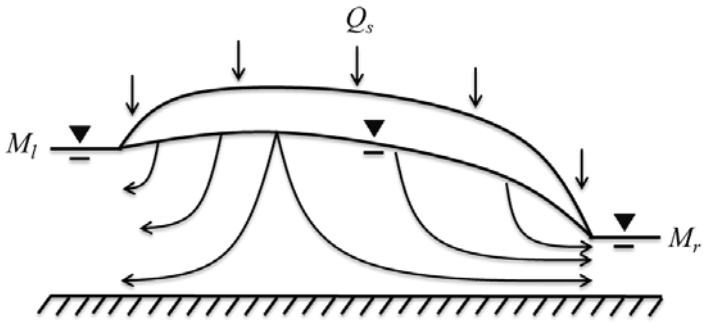

Figure 4. Schematic of a simple profile with Dirichlet boundary conditions on the right and left(M_r, M_r) a constant source (Q_s), and steady state variably saturated flow. In this case there exist a water divide in the domain. In the theory, the vertical and horizontal extent of the cross-section is assumed to be constant.

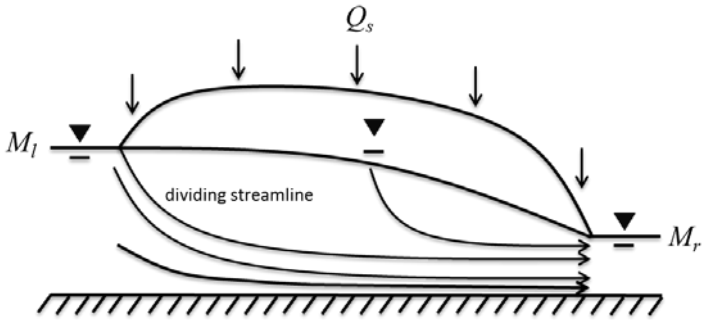

448

449 Figure 5. Schematic of a simple profile with Dirichlet boundary conditions on the right and left(M_r, M_r), a
450 constant source (Q_s), and steady state variably saturated groundwater flow. Note the dividing streamline
451 in this example. In the theory, the vertical and horizontal extents of the cross-section are assumed to be
452 constant.

453

454

455

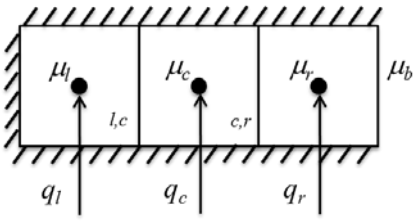

456

457 Figure 6. Schematic of the discrete example consisting of three microscale elements with a Dirichlet
458 boundary condition on the right side (μ_b) and a source/sink in each element (q_l, q_c, q_r).

459

460

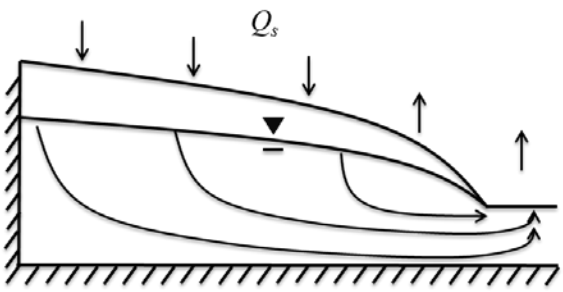

461

462 Figure 7. Schematic of a simple profile with a no-flow boundary condition on the left and right (based on

463 symmetry) and transient, spatially varying sources/sinks $Q_s(x,t)$ resulting in a recharge and discharge

464 area. In the theory, the vertical and horizontal extent of the cross-section is assumed to be constant.

465